ACS APPLIED MATERIALS & INTERFACES

Research Article

www.acsami.org

Influence of the Surface Structure of Graphene Oxide on the Adsorption of Aromatic Organic Compounds from Water

Han Yan, Hu Wu, Kun Li, Yawen Wang, Xue Tao, Hu Yang,* Aimin Li, and Rongshi Cheng

State Key Laboratory of Pollution Control and Resource Reuse, School of the Environment, School of Chemistry and Chemical Engineering, Nanjing University, Nanjing 210023, People's Republic of China

Supporting Information

ABSTRACT: In this work, graphene oxide (GO) has been employed as an efficient adsorbent for the removal of three aromatic organic compounds (AOCs), namely, aniline, nitrobenzene, and chlorobenzene, from water under various initial AOC concentrations and pH levels. Based on the characteristics of surface structures of GO, a simple semiquantitative model has been provided to describe the intrinsic adsorption behavior of GO to AOCs. Accordingly, the adsorption mechanism has been discussed in detail at molecular levels. The contribution coefficients derived from the proposed model indicate that the most preferential interactions between GO and AOCs are hydrophobic interactions ($\pi-\pi$ stacking and hydrophobic effect) that occur on graphitic zones of GO (unoxidized region). In the oxidized region, there also exist the hydrophobic interactions on sp^2 clusters, although they may be hindered by surrounding sp^3 zones which are the most unfavorable and are only accessible to AOCs through hydrogen bonding or electrostatic effects. More interestingly, aniline exhibits the highest contribution coefficients in both hydrophobic and hydrophilic zones of GO among the three measured AOCs due to its good water solubility and facile formation of hydrogen bonds. Furthermore, the analytical results of the adsorption isotherms are also fully consistent with those from the proposed model.

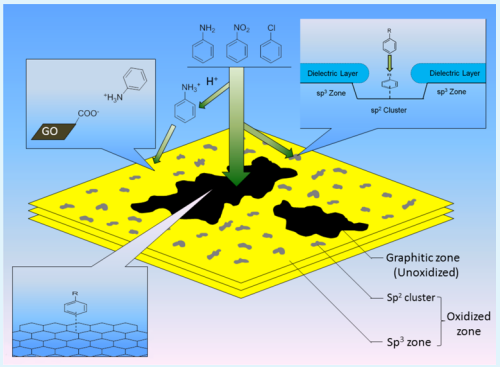

KEYWORDS: *graphene oxide, aromatic organic compounds, surface structure, semiquantitative adsorption model, adsorption mechanism*

1. INTRODUCTION

Graphene oxide (GO), a two-dimensional (2D) carbon-based nanomaterial with an atomic thickness and a large planar size, has received much more attention in terms of potential applications in various fields for its extraordinary structure and properties.[1−4] These exceptional advantages also endue GO with excellent performance in environmental remediation and water treatment as adsorbents, flocculants, environmental sensors, catalysts, and so on.[5−13] Among them, the high specific surface area (theoretical limit, 2630 $m^2\ g^{-1}$)[2] makes GO a potential superior adsorbent. In fact, GO has already shown significant efficiency for adsorption of many kinds of organic matters and metal ions from water.[14−16] Therefore, it is of great environmental importance to understand well the molecular interaction mechanisms between GO and the pollutants.

Besides the characteristics of the targeted contaminant itself, the interaction between GO and pollutants is closely related to the surface structure of the carbon-based materials, which is flexible and tunable.[17,18] The surface regions of GO usually consist of two parts:[19] unoxidized graphitic zones and oxidized zones. The former mainly exists in lowly oxidized or reduced GOs; the latter is made up of remnant sp^2 clusters and sp^3 zones, where the oxygen-containing functional groups have been introduced. The oxygen-containing functional groups tend to bind hydrophilic species due to ion exchange, hydrogen bonding or coordination effects,[20,21] whereas the aromatic clusters are affinitive to nonelectrolytic hydrophobic organic compounds by $\pi-\pi$ stacking or other hydrophobic interactions.[22,23] In addition, the sp^2 clusters in oxidized region are also facile to bind hydrophobic moieties, although they are partially hindered by the surrounding sp^3s.[24] Due to various zones of GO with far different adsorption affinity, the adsorption behavior of GO greatly depends on its surface structural feature. Therefore, it is crucial to study the molecular interaction mechanism between GO and pollutants in the adsorption process and further extend its application scope from the characteristics of the surface structure of GO. However, previous studies have mainly focused on the qualitative explanation and little work has been done in quantitative description.

It is well-known that most aromatic organic compounds (AOCs) are hazardous and dangerous to human and aquatic life;[23,25] therefore, efficient removal of these compounds from water is of great significance. In this work, five GO samples with different oxidation degrees and surface structural features have been prepared and employed in the removal of three AOCs

Received: January 4, 2015
Accepted: March 12, 2015
Published: March 12, 2015

DOI: 10.1021/acsami.5b00053
ACS Appl. Mater. Interfaces 2015, 7, 6690−6697

from water, namely, aniline (AN), nitrobenzene (NB), and chlorobenzene (CB). The adsorption performance of the GOs has been investigated systematically under various initial AOC concentrations and pH levels. Then, a simple semiquantitative model has been provided to describe the molecular interaction mechanisms of GO to AOCs based on the characteristics of surface structures of GO, and the adsorption mechanisms have been discussed in detail.

2. MATERIALS AND METHODS

2.1. Materials. The materials for preparation of GO (i.e., graphite, sulfuric acid, $KMnO_4$, sodium nitrate, and hydrogen peroxide) were all purchased from Nanjing Chemical Reagent Co., Ltd., China. Aniline, nitrobenzene, and chlorobenzene were obtained from Sinopharm Chemical Reagent Co., Ltd., China; the physiochemical parameters of these AOCs are listed in Table 1.[26−28] All the reagents are of analytical grade, and distilled water was used in all experiments.

Table 1. Physiochemical Parameters of Various AOCs.[26−28]

AOC	AN	NB	CB
molecular weight (g mol^{-1})	93.13	123.06	112.56
boiling point (°C)	184.1	210.9	131
solubility (g dm^{-3})	36	1.9	0.4
dipole moment	1.55	4.28	1.54
polarizability	0.73	1.01	2.7
pK_b	4.63		
hydrogen bonding acceptor constant	0.5	0.3	
hydrogen bonding donor constant	0.16		

2.2. Preparation of GOs with Different Oxidation Degrees. GOs with different oxidation degrees and surface structures were prepared according to Hummer's method[29] by adjusting the dose of the oxidant and the oxidation time.[18] $KMnO_4$ was used as the oxidant. The detailed preparation conditions are listed in Table 2.

2.3. Characterization of the Graphene Oxides. The structures of various GOs have been characterized by Raman spectroscopy (Type LabRAM Aramis; Horiba Co., Ltd., Japan) with 532 nm excitation wavelength, wide-angle X-ray diffraction (XRD, Type XRD-6000; Shimazu Co., Ltd., Japan) at a voltage of 40 kV and a current of 30 mA using Cu Kα radiation (λ = 0.15418 nm), and X-ray photoelectron spectroscopy (XPS, Type ULVAC-PHI 5000; VersaProbe, Northrop Grumman Co. Ltd.; USA).

Moreover, the content of surface oxygen-containing functional groups on GOs (i.e., carboxyl, lactonic, and phenolic groups) has been determined by Boehm titration[30] and the special surface area of each GO has been calculated by methylene blue titration,[31] which has been described in detail in the Supporting Information, texts S1 and S2, respectively.

2.4. Adsorption Experiments. *2.4.1. Effect of Initial Solution pH.* The effect of different initial solution pH on adsorption behavior of GOs for the removal of three AOCs (AN, NB, and CB) from aqueous solutions was studied at 298 K first. The initial solution pH of the AOC solutions ranged from 2.0 to 11.0 and was adjusted by dilute HCl or NaOH aqueous solutions. In this experiment, 0.015 g of each GO was first dispersed in a certain AOC aqueous solution. Then, the mixture was ultrasonicated for 5 min for full exfoliation. The initial concentration of each AOC solution was kept 1.0 mmol dm^{-3}. After the solution reached adsorption equilibrium, a desired amount was taken out and then underwent proper centrifugation and filtration to remove remnant GOs that would interfere with subsequent analyses. The concentration of the AOCs was analyzed using a UV−vis spectrometer (Agilent 8453). The analyzing wavelength was 230 nm for AN, 268 nm for NB, and 209 nm for CB. Proper dilution and pH adjustment were made to meet the analytical conditions if necessary.

Adsorption capacity (q, mg g^{-1}) of GO was calculated from the change of AOC concentration in the adsorption process on the basis of the following equation,

$$q = \frac{(C_0 - C_e)V}{m} \quad (1)$$

where C_0 and C_e (mg dm^{-3}) are the initial and equilibrium AOC concentrations of the AOC and GO aqueous mixture, respectively; V (dm^3) is the total volume of the solution at equilibrium; m (g) is the weight of GO.

2.4.2. Adsorption Equilibrium Study. The adsorption equilibrium study for the removal of various AOCs was conducted at 298 K and an initial solution pH 5.9. The concentrations of each series of AOC solution ranged from 10 to 125 mg dm^{-3}. First, 0.015 g of GO was dispersed and ultrasonicated under the same conditions described in section 2.4.1. An analysis method similar to the one mentioned above was employed to detect the initial and final AOC concentrations using a UV−vis spectrometer. The AOC uptakes were calculated on the basis of eq 1.

3. RESULTS AND DISCUSSION

3.1. Structural Characterizations of GO. Five GO samples with different surface structures and oxidation degrees have been prepared[18,29] and characterized by Raman, XRD, and XPS. The corresponding spectra are shown in Figure 1. From Raman spectra in Figure 1a, D and G bands at around 1340 and

Table 2. Preparation Conditions and Physiochemical Parameters of Graphite and the GO Series

sample	graphite	GO1	GO2	GO3	GO4	GO5
oxidation time at 305 K (min)	0	10	15	20	30	60
$KMnO_4$ dose (g)	0	6	9	12	15	15
aromatic cluster size (nm)[a]		1.94	1.87	1.72	1.63	1.32
content of graphitic zones (G%)[b]	0	77.3	49.7	6.2	∼0	∼0
content of sp^2 clusters in oxidized zones (a%)[c]	0	53.8	49.5	47.0	45.2	43.1
n_{total} (mmol g^{-1})[d]	0	1.8	3.2	5.0	5.3	5.8
n_{OH} (mmol g^{-1})[d]	0	1.0	2.1	2.7	2.8	3.1
$n_{lactonic}$ (mmol g^{-1})[d]	0	0.7	0.9	1.4	1.4	1.4
n_{COOH} (mmol g^{-1})[d]	0	<0.1	0.2	0.9	1.1	1.3
surface area (m^2 g^{-1})[e]	<10	40.0	80.0	4.0×10^2	6.7×10^2	7.5×10^2
A_1 (m^2 g^{-1})		30.9	39.8	24.8	0	0
A_2 (m^2 g^{-1})		4.9	19.9	176.3	302.8	323.2
A_3 (m^2 g^{-1})		4.2	20.3	198.8	367.2	426.8

[a]Calculated based on eq 2. [b]Calculated based on eq 3. [c]Calculated based on eq 4. [d]Obtained from Boehm titration results (detailed information available in Supporting Information, S1). [e]Estimated from methylene blue titration results (detailed information available in Supporting Information, S2).

DOI: 10.1021/acsami.5b00053
ACS Appl. Mater. Interfaces 2015, 7, 6690−6697

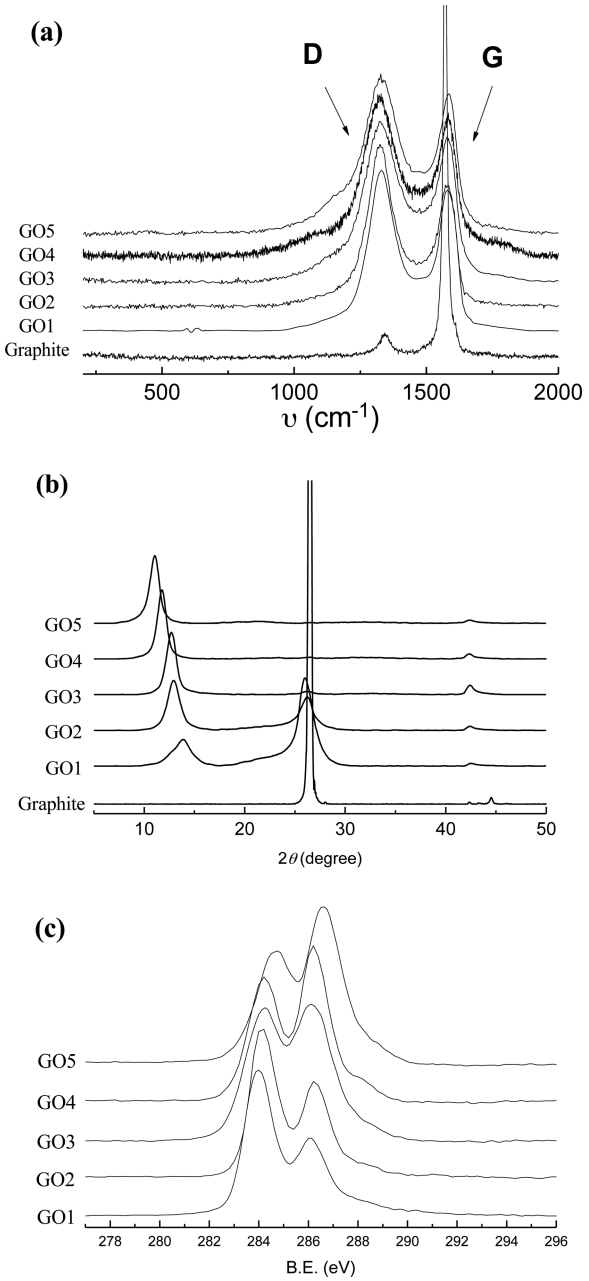

Figure 1. (a) Raman, (b) XRD, and (c) XPS spectra of the GO series.

1570 cm^{-1} associated with the sp^3 and sp^2 carbon atom vibration, respectively, are all observed in each GO. Accordingly, the aromatic cluster size in each GO is calculated based on the intensity ratio of G/D peaks by the empirical equation[32]

$$L = 4\frac{I_G}{I_D} \tag{2}$$

where L (nm) is the average aromatic cluster size; I_G and I_D are the integrated intensities of G and D peaks, respectively.

On the basis of XRD results shown in Figure 1b, we calculated the amount of graphitic zones (unoxidized region in GO; G%) using eq 3,

$$G\% = \frac{I_{Graphite}}{I_{GO} + I_{Graphite}} \times 100\% \tag{3}$$

where $I_{Graphite}$ and I_{GO} are the integrated intensities of graphitic (2θ = 27°) and oxidized peaks (2θ = 10−15°) in the XRD spectrum of GO,[33] respectively.

Figure 1c is the CXPS spectra of the GO series. Then the content of sp^2 clusters in oxidized zones of GO (a%) is calculated according to the XPS simulation results as shown in Figure S1 (Supporting Information) via eq 4,[34]

$$a\% = \frac{I_{sp^2}}{I_{total}} \times 100\% \tag{4}$$

where I_{sp^2} is the integrated intensity of sp^2 peak (B.E. = ∼284.5 eV) and I_{total} is the total integrated intensity of all the peaks in C 1s XPS spectrum of GO.

The obtained aromatic cluster size, content of graphitic zones in GO (G%), and content of sp^2 clusters in oxidized zones (a %) are all listed in Table 2. The aforementioned three parameters decrease with the increase of $KMnO_4$ dose and the oxidation time, while the oxygen-containing functional groups on GO determined by Boehm titration[30] and the special surface area of GO calculated by methylene blue titration[31] both increase, as can be seen from Table 2. They all illustrate that the unoxidized graphitic zone in GO decreases, but the oxidized zone increases from GO1 to GO5. Moreover, the surface morphologies of the graphite and various GO samples were observed directly by TEM, shown in Figure 2. The compact stacked multilayer planar carbon sheets are gradually changed to stretched few-layered ones from graphite to GO5. Above all, oxidation has greatly changed the surface structure of GO, of which the exfoliation degree and dispersibility in water have been both improved with increasing oxidation degree.

3.2. Adsorption Experiments. *3.2.1. Effect of Initial Solution pH.* Then the GOs were employed as adsorbents for the removal of AN, NB, and CB from aqueous solutions, respectively. The effects of initial solution pH have been conducted first and are shown in Figure 3. The adsorptions of three AOCs by GO exhibit different pH dependencies. The AN uptakes of GOs all show the up−climax−down variation trend, and the maximal adsorption capacities appear at pH between 5.0 and 9.0 (Figure 3a), while the adsorptions of NB and CB by each GO are all nearly pH independent (Figure 3b,c). This may be ascribed to different structural characteristics of three AOCs and various molecular adsorption mechanisms.

The three AOCs with aromatic structures all have high adsorption affinities to benzene rings of graphite zones in GOs by $\pi-\pi$ stacking and hydrophobic interactions,[22,23] the effects of which were not evidently influenced by pH. Therefore, the adsorption behavior of the GOs for both NB and CB exhibits pH independence. However, AN containing amino group has good water solubility and hydrogen bonding ability. The water solubility and the hydrogen bonding donor−acceptor parameters of AN (36 g dm^{-3} and 0.66, respectively) are both much higher than those of NB and CB, as can be seen from Table 1.[26−28] The formed cationic $-NH_3^+$ groups on AN through protonation can efficiently bind with anionic oxygen-containing functional groups of GO by electrostatic interactions.[35] Therefore, both hydrophilic and hydrophobic interaction mechanisms are involved in AN adsorption, which is different from NB and CB. However, the drop of AN uptakes in strong acidic solutions is due to the inhibition of hydrophilic interactions because most of AN is protonated, whereas the decrease in alkaline solutions is ascribed to the inhibition of the

DOI: 10.1021/acsami.5b00053
ACS Appl. Mater. Interfaces 2015, 7, 6690−6697

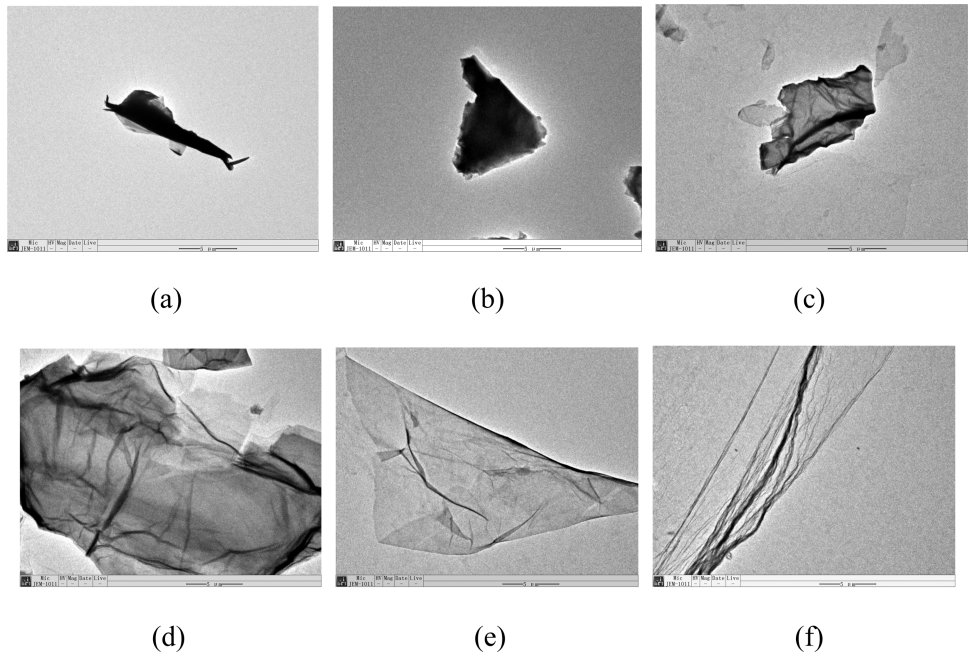

Figure 2. TEM images of the graphite and GO series: (a) graphite, (b) GO1, (c) GO2, (d) GO3, (e) GO4, and (f) GO5. The magnification in all images is 30000×.

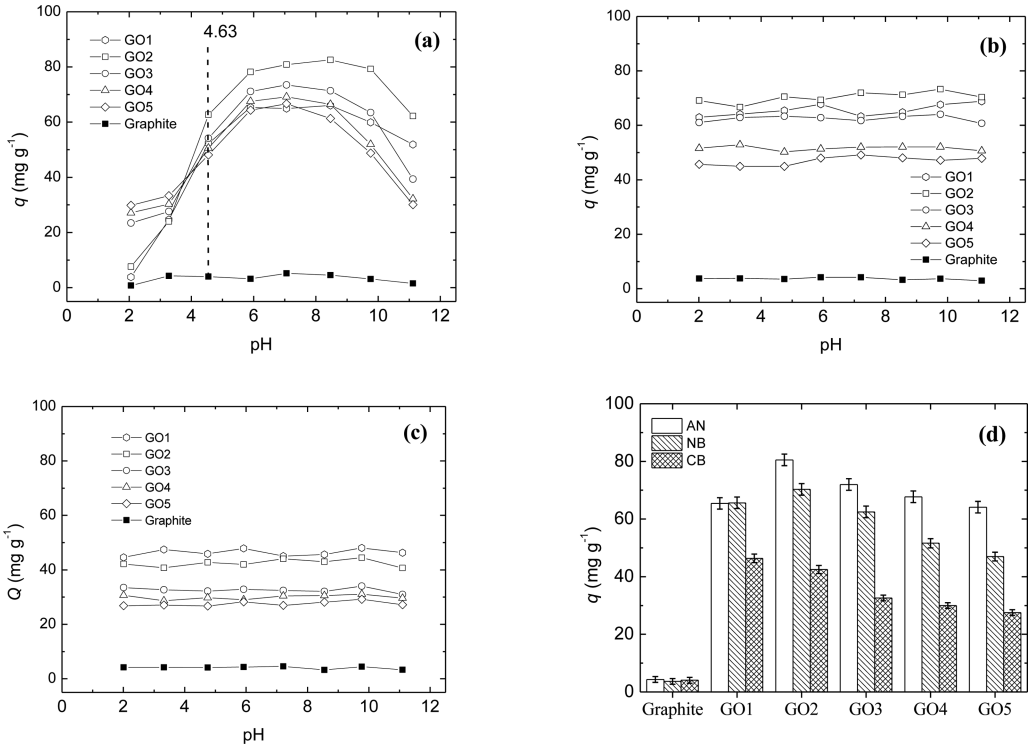

Figure 3. PH dependence of AOC uptakes of graphite and the GO series at 298 K: (a) AN, (b) NB, and (c) CB. (d) Average AOCs uptakes of graphite and the GO series at pH between 5.0 and 9.0. The initial solution concentration of each AOC is 1.0 mmol dm^{-3}.

hydrophobic interactions because most of the AN is deprotonated.

Interestingly, the AN uptakes at pH 2.0 increase with the increase of oxidation degree from GO1 to GO5, but those at pH 11.0 roughly decrease on the contrary, on the basis of Figure 3a, because the former is mainly due to increased hydrophilic interactions, while the latter is ascribed to enhanced hydrophobic interactions. Moreover, the AN uptake of each GO at low pH is smaller than its corresponding one at high pH. It indicates that hydrophobic interactions may have more contributions to AN removal, which may also result in an accelerated growth of the AN uptakes at pH 5.0 (Figure 3a) for a pK_b of AN of approximately 4.63.[27]

The average AOC uptakes of graphite and the GO series at pH between 5.0 and 9.0 have been summarized in Figure 3d according to Figure 3a–c. As can be observed, graphite always

DOI: 10.1021/acsami.5b00053
ACS Appl. Mater. Interfaces 2015, 7, 6690–6697

exhibits the lowest AOCs removal efficiency due to its low surface area and lack of activated adsorption sites. From Figure 2a, graphite is hardly dispersible and facile to form large aggregates in water for its hydrophobic surface structure. Interestingly, the special surface area and water dispersibility of GO increase with increasing oxidation degree based on Table 2 and Figure 2, but the AOC uptakes could not increase simultaneously. From Figure 3d, GO1 and GO2 with relatively low oxidation degree bear higher AOC removal efficiency, and AOC uptakes would further decrease with the increase of oxidation degree. It is due to the fact that the hydrophobic interactions are dominant in AOC adsorption. Although the special surface area and dispersibility of GO both increase from GO1 to GO5, the total oxidized zones in GO also increase at the same time, resulting in the reduction of the effective activated adsorption sites. Therefore, there are two opposite effects on AOC removal for GO by increasing oxidation degree, and GO with suitable oxidation degree bears high AOC removal efficiency.

Moreover, for different AOCs, the maximal adsorption capacities is in the order of AN > NB > CB from Figure 3d, which is consistent with their solubility.[26−28] Although the hydrophobic interactions play major roles in the adsorption process,[13−16,23,36] better water solubility of AOCs would make additional contributions: On the one hand, hydrophilic interactions between AOC and oxygen-containing functional groups on GO, especially for AN, would take place;[37] on the other hand, good water solubility would be beneficial to accelerate the diffusion or migration rate of the AOC from bulk solution to GO's surface to achieve adsorption efficiently.

3.2.2. Equilibrium Adsorption Experiments. Subsequently, the equilibrium adsorption isotherms are illustrated in Figure 4. AOC uptakes of the GO series increase linearly with increasing the AOC concentrations at the beginning, then reach to surface saturation at high concentrations.

For further analysis, those results were subjected to Langmuir and Freundlich isothermal models,[38,39] which suggest monolayer homogeneous and multilayer heterogeneous adsorptions, respectively. Their equations are shown below:

$$\frac{C_e}{q_e} = \frac{1}{q_m b} + \frac{C_e}{q_m} \quad (5)$$

$$\log q_e = \frac{1}{n}\log(C_e) + \log K_f \quad (6)$$

where q_e is the amount of AOC adsorbed at equilibrium (mg g^{-1}); C_e is the AOC concentration at equilibrium (mg dm^{-3}); q_m is the adsorption capacity when the adsorbent is fully covered (mg g^{-1}); b is the Langmuir adsorption constant (dm^3 mg^{-1}); K_f is the Freundlich isothermal constant, and n (dimensionless) is the heterogeneity factor. The simulation results are all listed in Table 3.

On the basis of the correlation coefficients (R^2), Freundlich model could describe the isothermal adsorption behavior of the GOs for removal of these three AOCs all better than Langmuir model. It indicates that multilayer heterogeneous adsorption is dominant due to the hydrophobic interactions, which well agrees with the results as discussed in the previous section, and the adsorption behavior of most aromatic organic compounds.[40,41] More interestingly, the variation trends of the Freundlich parameter (K) illuminating the favorability of the adsorption process are also fully consistent with those of adsorption capacities from GO1 to GO5 in all of the three

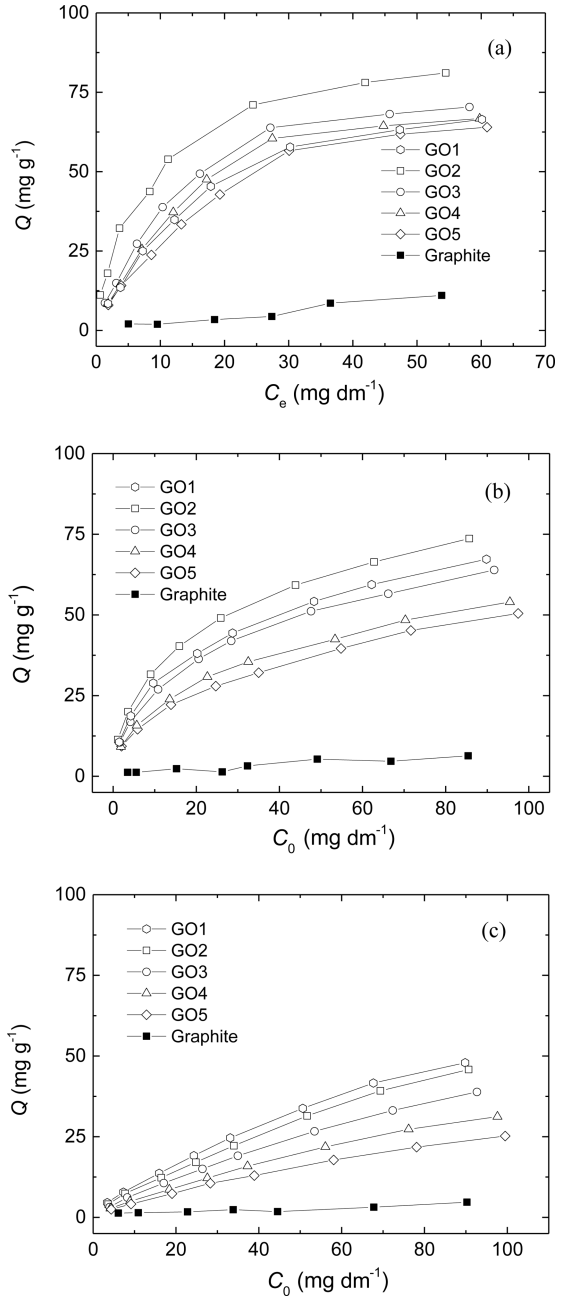

Figure 4. AOCs uptakes of the GO series versus various equilibrium solution concentrations of AOCs at 298 K and pH 5.9: (a) AN, (b) NB, and (c) CB.

AOCs systems according to Table 3 and Figure 3d. It has further confirmed that the AOCs adsorptions by GOs mainly obey Freundlich model.

However, the R^2s of the Langmuir model for each GO in the AN system are also quite high, indicating that monolayer homogeneous adsorption may also be involved in AN removal ascribed to hydrophilic interactions. Moreover, the larger deviation from Langmuir model for CB adsorption on the basis of Table 3 suggests that the multilayer and heterogeneous adsorption is more dominant in CB due to its higher hydrophobic effect.[42]

3.3. AOC Adsorption Models. The above discussion about the adsorption mechanism still basically depends on qualitative description. A quantitative characterization that offers further

DOI: 10.1021/acsami.5b00053
ACS Appl. Mater. Interfaces 2015, 7, 6690−6697

Table 3. Isothermal Parameters for Adsorption of Various AOCs onto the GO Series at 298 K and pH 5.9

model	AOC		GO1	GO2	GO3	GO4	GO5
Langmuir	AN	q_m (mg g^{-1})	99.8	86.8	102.3	115.1	98.6
		b (10^{-2}dm mg^{-1})	4.5	15.9	5.9	4.0	4.1
		R^2	0.9788	0.9715	0.9795	0.9898	0.9484
	NB	q_m (mg g^{-1})	63.1	68.7	60.8	50.5	46.2
		b (10^{-2}dm mg^{-1})	9.6	11.2	8.8	8.0	7.8
		R^2	0.9775	0.9767	0.9747	0.9768	0.9633
	CB	q_m (mg g^{-1})	67.2	65.8	65.3	53.1	38.9
		b (10^{-2}dm mg^{-1})	1.80	1.57	1.21	1.16	1.34
		R^2	0.8599	0.8264	0. 9134	0.8454	0.8767
Freundlich	AN	K	5.6	14.4	7.1	5.5	5.2
		n	1.40	1.91	1.45	1.33	1.41
		R^2	0.9885	0.9836	0.9906	0.9928	0.9985
	NB	K	9.3	11.1	8.5	6.9	6.8
		n	2.14	2.19	2.16	2.15	2.28
		R^2	0.9929	0.9961	0.9977	0.9971	0.9991
	CB	K	1.80	1.53	1.07	0.87	0.78
		n	1.35	1.32	1.23	1.25	1.30
		R^2	0.9990	0.9983	0.9989	0.9993	0.9981

details is more significant. As is known, the AOCs interact with GO mainly through two pathways, that is, hydrophobic and hydrophilic interactions.[13−16,23] On the basis of the characteristics of the GO's surface structure, hydrophobic interactions would take place at unoxidized graphitic zones and sp^2 zone of the oxidized parts in GO, whereas hydrophilic interactions exist on sp^3 zones of the oxidized regions. Furthermore, the combination of the obtained special surface area (S, m^2 g^{-1}), the content of graphitic zones in GO (G%), and the content of sp^2 clusters in oxidized zones (a%), all listed in Table 2, the area of graphitic zones (A_1, m^2 g^{-1}), the area of the sp^2 clusters (A_2, m^2 g^{-1}), and sp^3 zones (A_3, m^2 g^{-1}) in oxidized regions could be roughly estimated from the following equations.

$$A_1 = SG\% \tag{7}$$

$$A_2 = S(1 - G\%)a\% \tag{8}$$

$$A_3 = S(1 - G\%)(1 - a\%) \tag{9}$$

It is assumed that AOCs adsorption by GO obeys a simple accumulation of the contributions from the aforementioned zones. A simple model has been deduced to evaluate the adsorption behavior and molecular interaction mechanism, which is shown below,

$$q = aA_1 + bA_2 + cA_3 \tag{10}$$

where q (mg g^{-1}) is the adsorption capacity of GO; a, b, and c (mg m^{-2}) are the contribution coefficients of the corresponding zones in GO and also describe the adsorption density of each region, which is associated with the water solubility of pollutants, π-electron polarity/polarizability, and hydrogen bonding donor−acceptor parameters.[13−16,23]

On the basis of eq 10, the simulation results are listed in Table 4. The contribution coefficients for each AOC follow the order of $a \gg b > c$. The parameter of a corresponding to hydrophobic interactions in graphitic zones is much greater than the other two, indicating that the graphitic zone in GO plays a major role in AOCs adsorption. Moreover, the contribution from sp^2 clusters in oxidized regions (b) is more than that from sp^3 zones (c) but much less than that from graphitic regions (a) on the basis of Table 4, suggesting that hydrophobic interactions are more favorable even in oxidized regions. The coefficient corresponding to sp^2 clusters (b) is much lower than that to graphitic zones (a), which is due to the hindrance effects by surrounding sp^3 zones,[24] although there lies similar adsorption mechanism in these two hydrophobic regions. The sp^3 zones are easy to be solvated and form dielectric layers, which would hinder AOCs from approaching GO's surface, making it incapable to achieve adsorption through hydrophobic interactions. From GO3 to GO5, increased oxidation degree results in enhanced hindrance effects and reduction of the effective activated adsorption sites, which is responsible for the decrease of each AOC uptake according to Figure 3d, although the apparent area of sp^2 clusters in oxidized region (A_2) increase simultaneously (Table 2). Furthermore, the hydrophilic sp^3 zones are the most unfavorable to AOCs because they interact with AOCs only through hydrogen bonding or electrostatic effects. On the basis of the previous discussion, the detailed adsorption mechanisms of GO for AOCs removal are summarized and demonstrated in Scheme 1.

Table 4. Contribution Coefficients of Different Zones in GO for Adsorption of Various AOCs at 298 K and pH 5.9

AOC	AN	NB	CB
a (mg m^{-2})	1.88	1.82	1.22
b (10^{-2} mg m^{-2})	9.76	9.63	6.85
c (10^{-2} mg m^{-2})	7.91	4.35	0.97
R^2	0.9799	0.9771	0.9394

Moreover, in comparison with each contribution coefficient among the three AOCs, the a, b, and c values all follow the order of AN > NB > CB. It is reasonable that the coefficient of c related to hydrophilic interactions obeys the aforementioned order, because it is fully consistent with the hydrophilicity of the three AOCs. The hydrogen bonding donor−acceptor parameters are 0.66, 0.3, and 0 for AN, NB, and CB, respectively.[26−28] The inability to form hydrogen bonds for CB results in near zero of its c value, indicating that CB is extremely unfavorable to hydrophilic sites on GO.

However, as for parameters a and b, both related to hydrophobic interactions, those of AN are also the highest ones among the three AOCs, despite its lowest hydrophobicity. It

DOI: 10.1021/acsami.5b00053
ACS Appl. Mater. Interfaces 2015, 7, 6690−6697

Scheme 1. Summarized Adsorption Mechanisms of GO for Removal of AOCs from Water

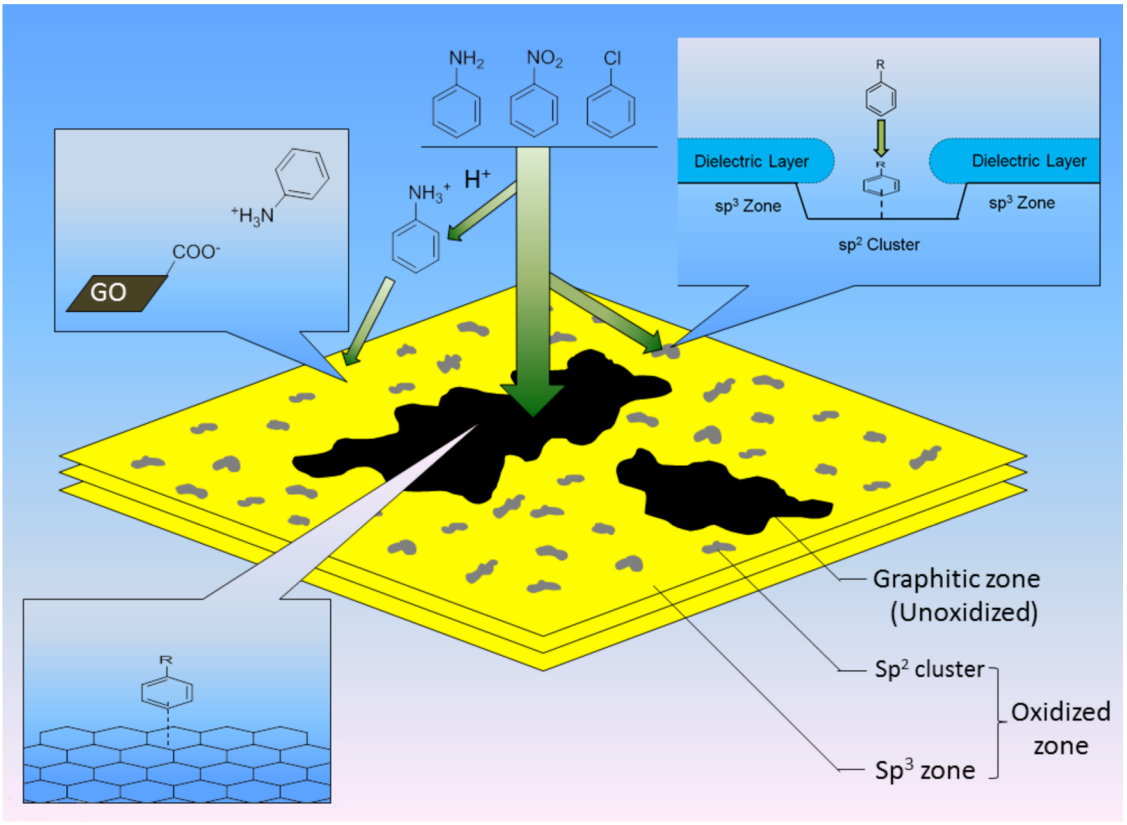

illuminates that the promoted diffusion or migration rate of AN in solution for its good water solubility have positive effects to access to hydrophobic sites and achieve adsorption. Moreover, the relative differences between AN and NB in both *a* and *b* values are much smaller than that in *c* from Table 4. Both *a* and *b* values of NB are much closer to those of AN resulting from the higher hydrophobicity of NB, which may partly compensate its lower migration rate in water.

4. CONCLUSION

In this current work, the adsorption behavior of GO for the removal of three AOCs (AN, NB, and CB) from water was studied. A simple semiquantitative model has been developed based on the characteristics of surface structure of GO. The theoretical results are in desirable agreement with the experimental facts. The hydrophobic interactions ($\pi-\pi$ stacking and hydrophobic effects) between GO and AOCs are dominant in whole adsorption process. Therefore, moderately oxidized GO bears enhanced adsorption performance for AOCs removal due to its good dispersibility and adequate activated adsorption sites. Moreover, this model has been built by fully considering various contributions from structural factors of GO and different effects including hydrophobic and hydrophilic interactions. Accordingly, on the one hand, it has properly explained the diverse contributions to AOC adsorption from different zones on GO with distinct surface structures, as well as the different removal efficiency among three AOCs essentially caused by their different structural characteristics. On the other hand, it is potentially capable of evaluating the adsorption behavior of GO for the removal of other pollutants such as heavy metal ions, water-soluble organic compounds, and so on. As a result, the proper GO-based adsorbents could be designed or selected successfully on the basis of the characteristics of targeted contaminants and structure–activity relationship, which is significant for their practical application potentials.

■ ASSOCIATED CONTENT

Supporting Information

The procedures of Boehm titration of GOs (Text S1) and their surface area determination by methylene blue titration (Text S2). Line shape analysis for the C1s XPS spectra of the GOs. (Figure S1). This material is available free of charge via the Internet at http://pubs.acs.org.

■ AUTHOR INFORMATION

Corresponding Author

*Tel./Fax: 86-25-89681272. E-mail: yanghu@nju.edu.cn.

Notes

The authors declare no competing financial interest.

■ ACKNOWLEDGMENTS

This work was supported by the Natural Science Foundation of China (Grant Nos. 51438008 and 51378250).

■ REFERENCES

(1) Allen, M. J.; Tung, V. C.; Kaner, R. B. Honeycomb Carbon: A Review of Graphene. *Chem. Rev.* **2009**, *110* (1), 132–145.

(2) Zhu, Y.; Murali, S.; Cai, W.; Li, X.; Suk, J. W.; Potts, J. R.; Ruoff, R. S. Graphene and Graphene Oxide: Synthesis, Properties, and Applications. *Adv. Mater.* **2010**, *22* (35), 3906–3924.

(3) Wang, J.; Tsuzuki, T.; Tang, B.; Hou, X.; Sun, L.; Wang, X. Reduced Graphene Oxide/ZnO Composite: Reusable Adsorbent for Pollutant Management. *ACS Appl. Mater. Interfaces* **2012**, *4* (6), 3084–3090.

DOI: 10.1021/acsami.5b00053
ACS Appl. Mater. Interfaces 2015, 7, 6690–6697

(4) Chen, D.; Feng, H.; Li, J. Graphene Oxide: Preparation, Functionalization, and Electrochemical Applications. *Chem. Rev.* **2012**, *112* (11), 6027−53.
(5) Yan, H.; Li, H.; Tao, X.; Li, K.; Yang, H.; Li, A.; Xiao, S.; Cheng, R. Rapid Removal and Separation Of Iron(II) And Manganese(II) from Micropolluted Water using Magnetic Graphene Oxide. *ACS Appl. Mater. Interfaces* **2014**, *6* (12), 9871−80.
(6) Yang, Z.; Yan, H.; Yang, H.; Li, H.; Li, A.; Cheng, R. Flocculation Performance and Mechanism of Graphene Oxide for Removal of Various Contaminants from Water. *Water Res.* **2013**, *47* (9), 3037−46.
(7) Simate, G. S.; Iyuke, S. E.; Ndlovu, S.; Heydenrych, M. The Heterogeneous Coagulation and Flocculation of Brewery Wastewater using Carbon Nanotubes. *Water Res.* **2012**, *46* (4), 1185−97.
(8) Huang, X.; Wang, L.; Zhou, J.; Gao, N. Photocatalytic Decomposition of Bromate Ion by the UV/P25-Graphene Processes. *Water Res.* **2014**, *57*, 1−7.
(9) Zhang, Z.; Xiao, F.; Guo, Y.; Wang, S.; Liu, Y. One-Pot Self-Assembled Three-Dimensional TiO_2-Graphene Hydrogel with Improved Adsorption Capacities and Photocatalytic and Electrochemical Activities. *ACS Appl. Mater. Interfaces* **2013**, *5* (6), 2227−2233.
(10) Zhao, G.; Li, J.; Ren, X.; Chen, C.; Wang, X. Few-Layered Graphene Oxide Nanosheets as Superior Sorbents for Heavy Metal Ion Pollution Management. *Environ. Sci. Technol.* **2011**, *45* (24), 10454−62.
(11) Zhao, G.; Jiang, L.; He, Y.; Li, J.; Dong, H.; Wang, X.; Hu, W. Sulfonated Graphene for Persistent Aromatic Pollutant Management. *Adv. Mater.* **2011**, *23* (34), 3959−3963.
(12) Chang, J.; Zhou, G.; Christensen, E.; Heideman, R.; Chen, J. Graphene-Based Sensors for Detection of Heavy Metals in Water: A Review. *Anal. Bioanal. Chem.* **2014**, *406* (16), 3957−3975.
(13) Zhao, G.; Wen, T.; Chen, C.; Wang, X. Synthesis Of Graphene-based Nanomaterials and Their Application in Energy-Related and Environmental-Related Areas. *RSC Adv.* **2012**, *2* (25), 9286.
(14) Wang, S.; Sun, H.; Ang, H. M.; Tadé, M. O. Adsorptive Remediation of Environmental Pollutants using Novel Graphene-Based Nanomaterials. *Chem. Eng. J.* **2013**, *226*, 336−347.
(15) Chowdhury, S.; Balasubramanian, R. Recent Advances in the Use of Graphene-Family Nanoadsorbents for Removal of Toxic Pollutants from Wastewater. *Adv. Colloid Interface Sci.* **2014**, *204*, 35−56.
(16) Zhao, J.; Wang, Z.; White, J. C.; Xing, B. Graphene in the Aquatic Environment: Adsorption, Dispersion, Toxicity, and Transformation. *Environ. Sci. Technol.* **2014**, *48* (17), 9995−10009.
(17) Compton, O. C.; Nguyen, S. T. Graphene Oxide, Highly Reduced Graphene Oxide, and Graphene: Versatile Building Blocks for Carbon-based Materials. *Small* **2010**, *6* (6), 711−23.
(18) Yan, H.; Tao, X.; Yang, Z.; Li, K.; Yang, H.; Li, A.; Cheng, R. Effects of the Oxidation Degree of Graphene Oxide on the Adsorption of Methylene Blue. *J. Hazard. Mater.* **2014**, *268*, 191−8.
(19) Dreyer, D. R.; Todd, A. D.; Bielawski, C. W. Harnessing the Chemistry of Graphene Oxide. *Chem. Soc. Rev.* **2014**, *43* (15), 5288−301.
(20) Sun, Y.; Wang, Q.; Chen, C.; Tan, X.; Wang, X. Interaction between Eu(III) and Graphene Oxide Nanosheets Investigated by Batch and Extended X-Ray Absorption Fine Structure Spectroscopy and By Modeling Techniques. *Environ. Sci. Technol.* **2012**, *46* (11), 6020−7.
(21) Fan, L.; Luo, C.; Sun, M.; Li, X.; Lu, F.; Qiu, H. Preparation of Novel Magnetic Chitosan/Graphene Oxide Composite as Effective Adsorbents toward Methylene Blue. *Bioresour. Technol.* **2012**, *114*, 703−6.
(22) Gomez-Navarro, C.; Meyer, J. C.; Sundaram, R. S.; Chuvilin, A.; Kurasch, S.; Burghard, M.; Kern, K.; Kaiser, U. Atomic Structure of Reduced Graphene Oxide. *Nano Lett.* **2010**, *10* (4), 1144−1148.
(23) Yang, K.; Xing, B. Adsorption of Organic Compounds by Carbon Nanomaterials in Aqueous Phase: Polanyi Theory and Its Application. *Chem. Rev.* **2010**, *110* (10), 5989−6008.
(24) Pendolino, F.; Parisini, E.; Lo Russo, S. Time-Dependent Structure and Solubilization Kinetics of Graphene Oxide in Methanol and Water Dispersions. *J. Phys. Chem. C* **2014**, *118* (48), 28162−28169.
(25) Lee, J. H.; Landrum, P. F. Application of Multi-Component Damage Assessment Model (MDAM) for the Toxicity of Metabolized PAH in Hyalella Azteca. *Environ. Sci. Technol.* **2006**, *40* (4), 1350−1357.
(26) Marcus, Y. Linear Solvation Energy Relationships. Correlation and Prediction of the Distribution of Organic Solutes between Water and Immiscible Organic Solvents. *J. Phys. Chem.* **1991**, *95*, 8886−8891.
(27) Dean, J. A. *Lange's Handbook of Chemistry*; McGraw-Hill: New York, 1999.
(28) Yang, K.; Wu, W.; Jing, Q.; Zhu, L. Aqueous Adsorption of Aniline, Phenol, and their Substitutes by Multi-Walled Carbon Nanotubes. *Environ. Sci. Technol.* **2008**, *42* (21), 7931−7936.
(29) Hummers, W. S. J.; Offeman, R. E. Preparation of Graphitic Oxide. *J. Am. Chem. Soc.* **1958**, *80*, 1339.
(30) Boehm, H. P. Some Aspects of the Surface Chemistry of Carbon Blacks and Other Carbons. *Carbon* **1994**, *32* (5), 759−769.
(31) Montes-Navajas, P.; Asenjo, N. G.; Santamaría, R.; Menéndez, R.; Corma, A.; García, H. Surface Area Measurement of Graphene Oxide in Aqueous Solutions. *Langmuir* **2013**, *29* (44), 13443−13448.
(32) Tuinstra, F. Raman Spectrum of Graphite. *J. Chem. Phys.* **1970**, *53* (3), 1126−1130.
(33) Talyzin, A. V.; Hausmaninger, T.; You, S.; Szabo, T. The Structure of Graphene Oxide Membranes in Liquid Water, Ethanol and Water-Ethanol Mixtures. *Nanoscale* **2014**, *6* (1), 272−281.
(34) Mattevi, C.; Eda, G.; Agnoli, S.; Miller, S.; Mkhoyan, K. A.; Celik, O.; Mastrogiovanni, D.; Granozzi, G.; Garfunkel, E.; Chhowalla, M. Evolution of Electrical, Chemical, and Structural Properties of Transparent and Conducting Chemically Derived Graphene Thin Films. *Adv. Funct. Mater.* **2009**, *19* (16), 2577−2583.
(35) Gao, W.; Alemany, L. B.; Ci, L.; Ajayan, P. M. New Insights into the Structure and Reduction of Graphite Oxide. *Nat. Chem.* **2009**, *1* (5), 403−408.
(36) Wang, J.; Chen, Z.; Chen, B. Adsorption of Polycyclic Aromatic Hydrocarbons by Graphene and Graphene Oxide Nanosheets. *Environ. Sci. Technol.* **2014**, *48* (9), 4817−4825.
(37) Park, J. S.; Goo, N. I.; Kim, D. E. Mechanism of DNA Adsorption and Desorption on Graphene Oxide. *Langmuir* **2014**, *30* (42), 12587−12595.
(38) Langmuir, I. The Adsorption of Gases on Plane Surfaces of Glass, Mica, and Platinum. *J. Am. Chem. Soc.* **1918**, *40*, 1361−1403.
(39) Freundlich, H. Ueber die Adsorption in Loesun. *Z. Phys. Chem.* **1907**, *57*, 385−470.
(40) Kragulj, M.; Tričković, J.; Dalmacija, B.; Kukovecz, Á.; Kónya, Z.; Molnar, J.; Rončević, S. Molecular Interactions between Organic Compounds and Functionally Modified Multiwalled Carbon Nanotubes. *Chem. Eng. J.* **2013**, *225*, 144−152.
(41) Pei, Z.; Li, L.; Sun, L.; Zhang, S.; Shan, X. Q.; Yang, S.; Wen, B. Adsorption Characteristics of 1,2,4-Trichlorobenzene, 2,4,6-Trichlorophenol, 2-Naphthol and Naphthalene on Graphene and Graphene Oxide. *Carbon* **2013**, *51*, 156−163.
(42) Chandler, D. Interfaces and the Driving Force of Hydrophobic Assembly. *Nature* **2005**, *437* (7059), 640−647.

DOI: 10.1021/acsami.5b00053
ACS Appl. Mater. Interfaces 2015, 7, 6690−6697